Journal of. Modern Trends in Physics Research
Online ISSN 2636-4220
DOI: 10.19138/mtpr/(14)81-89
Accepted: 2014-12-19

Structural and multiferroic properties of nanostructured barium doped Bismuth Ferrite

M. A. Ahmed[1], M. S. Ayoub[2], M. M. Mostafa[2], M. M. El–Desoky[2]

[1] *Materials Science Lab (1), Physics Department, Faculty of Science, Cairo University, Giza, Egypt*
[2] *Physics Department, Faculty of Science, Suez University, Suez, Egypt.*

Abstract- Multiferroic nanoparticles of $Bi_{1-x}Ba_xFeO_3$ (x = 0.10, 0.15, 0.20 and 0.25 mol%) samples were prepared using conventional solid-state method. The nanostructural, multiferroic properties of the prepared samples were investigated. X-ray diffraction (XRD) patterns show the formation of $BiBaFeO_3$ with single-phase rhombohedral-hexagonal structure. Spin canting or impurity phase could be a probable reason for the origin of ferromagnetism. At room temperature, remnant magnetization increased 18 times more than its initial value. A change in the magnetization is observed around 742–833 K. Néel temperature (T_N) registers an increase of 30 times of Ba-doped $BiFeO_3$ in comparison with undoped $BiFeO_3$. The dielectric properties were affected by the properties of the substitutional ions as well as the crystalline structure of the present samples. Substitution with Ba^{2+} ions also improved the ferroelectric polarization with remanent magnetization polarization of 89 $\mu C/cm^2$. The simultaneous occurrence of ferromagnetism and ferroelectric hysteresis loops in $BiBaFeO_3$ multiferroic nanoparticles system at room temperature makes it a potential candidate for information storage and spintronics.

Correspondence Author –M. M. El-Desoky: (mmdesoky@gmail.com)

Keywords- Density functional theory; Full Potential Linearized Augmented Plane Waves; spin polarized calculations; Generalized Gradient Approximation.

1. INTRODUCTION

Multiferroic materials are defined as single-phase crystals exhibiting both anti/ferromagnetism, anti/ferroelectricity and/or ferroelastic (hysteretic stress–strain relationships) at the same temperature and pressure [1]. Multiferroics have a wide range of potential applications in magnetic data storage, logic devices, spintronic devices, and sensors [2–3] as the coupling between magnetic and ferroelectric properties enables the dynamic interaction between these order parameters [4]. Magnetoelectric multiferroics that simultaneously show magnetic and ferroelectric order, such as $BiFeO_3$, are extensively studied for coupling between electric and magnetic order parameters [5–6].

$BiFeO_3$ is one of single-phase multiferroic materials with a distorted perovskite structure ABO_3 [7] and its ferroelectric, antiferromagnetic with a Curie temperature of ~1093 K and a Néel temperature of ~643 K [8] and it is still the only compound with coexisting of ferroelectricity and antiferromagnetism at room temperature [9]. It is one of the most studied multiferroics, because of its large polarization and its possible coupling with the magnetic moment [5, 10].

The impurities, large leakage current and antiferromagnetic nature are big barriers in applications of $BiFeO_3$ [11] and it is very difficult to obtain a single phase $BiFeO_3$ by using solid-state reaction at high sintering temperature [12]. In order to overcome these problems, doping method was considered best way to enhance multiferroic property through suppressing its cycloid structure or reducing the second phase [13]. So, the ferroelectric and magnetic properties of $BiFeO_3$ could be improved by substitution such as (Ca^{2+}, Sr^{2+}, Ba^{2+}, Mg^{2+}, Pb^{2+}) cations at Bi^{3+} site and

Journal of. Modern Trends in Physics Research
Online ISSN 2636-4220
DOI: 10.19138/mtpr/(14)81-89
Accepted: 2014-12-19

by (Co^{3+}, Cr^{3+}, Mn^{3+}, Ti^{4+}, V^{5+}, Nb^{5+}) cations at Fe^{3+} site [14–16]. These substitutions lead to improve the magnetic properties and change in crystal symmetry of $BiFeO_3$. Doping at A–site affects the centrosymmetry of FeO_6 octahedra, create oxygen vacancies, and lead to change multiferroic properties of $BiFeO_3$. Furthermore, the leakage currents reduced by Ba^{2+} ions doping [17–18].

In the present work, we have synthesized $Bi_{1-x}Ba_xFeO_3$ ($0.10 \le x \le 0.25$ mol%) multiferroic nanoparticles and investigated on the effect of Ba^{2+} ions substitution on the structural, dielectric, magnetic, ferroelectric and ferromagnetic properties of $BiFeO_3$ sample.

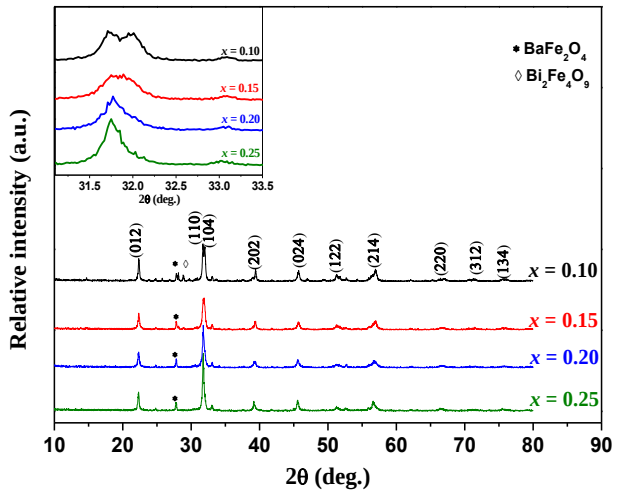

Fig.1 X-ray diffraction pattern for $Bi_{1-x}Ba_xFeO_3$ multiferroic nanoparticles at room temperature

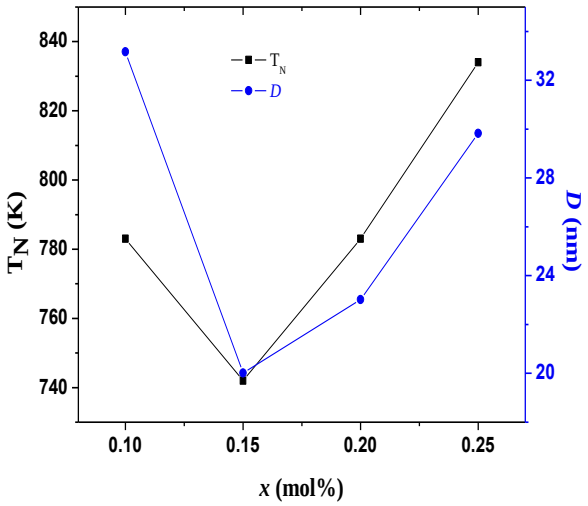

Fig.3 Dependence of the Néel temperature (T_N) and crystallite size (D) on the barium content (x).

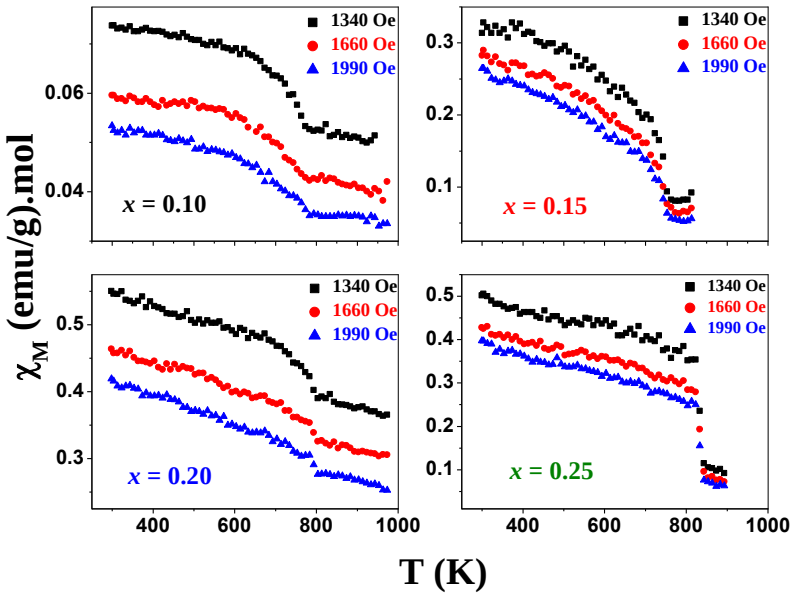

Journal of. Modern Trends in Physics Research
Online ISSN 2636-4220
DOI: 10.19138/mtpr/(14)81-89
Accepted: 2014-12-19

Fig.2 Dependence of the molar magnetic susceptibility (χ_M) on the absolute temperature (T) for $Bi_{1-x}Ba_xFeO_3$ multiferroic nanoparticles at different magnetic field intensities (H).

2. EXPERIMENTAL

Nanometric samples with having the chemical formula $Bi_{1-x}Ba_xFeO_3$; (x = 0.10, 0.15, 0.20 and 0.25 mol%) were prepared by the conventional solid-state reaction from analar grade form oxides (BDH), including Bi_2O_3, $BaCO_3$ and Fe_2O_3. Stoichiometric ratios of pure oxides, with purity 99.99%, were good mixed and grinded using agate mortar for 3.5 h. The samples were pressed into pellet form using uniaxial press. Presintering was carried out in air at 600 °C for 6 h using a heating rate of 4 °C/min. The samples were cooled to room temperature with the same above rate; regrinded for 1.5 h. Final sintering was carried out at 850 °C for 3 h with the same above rate in open atmosphere. The prepared samples were checked by X-ray diffraction using Diano corporation of target Co-Kα (λ= 1.79026Å) to assure the complete reaction and the formation of single-phase structure. The morphologies of the synthesized $BiBaFeO_3$ nanoparticle samples were observed by a scanning electron microscopy (SEM) (A Quanta 250 FEG, FEI Company). Transmission electron microscope (TEM) photographs were taken using TEM model (JEOL–1010). The dc magnetic susceptibility measurements were performed using Faraday's method from room temperature up to about 1000 K at three different values of magnetic field intensity ranging from 1340 Oe to 1990 Oe. The hysteresis and magnetization measurements were performed using vibrating sample magnetometer (VSM; 9600–1 LDJ, USA) with a maximum applied field of 20 kOe at room temperature. The polarization versus electric field (P–E) hysteresis loops were obtained at 300 K. Ferroelectric hysteresis loops were measured by using a Sawyer–Tower circuit.

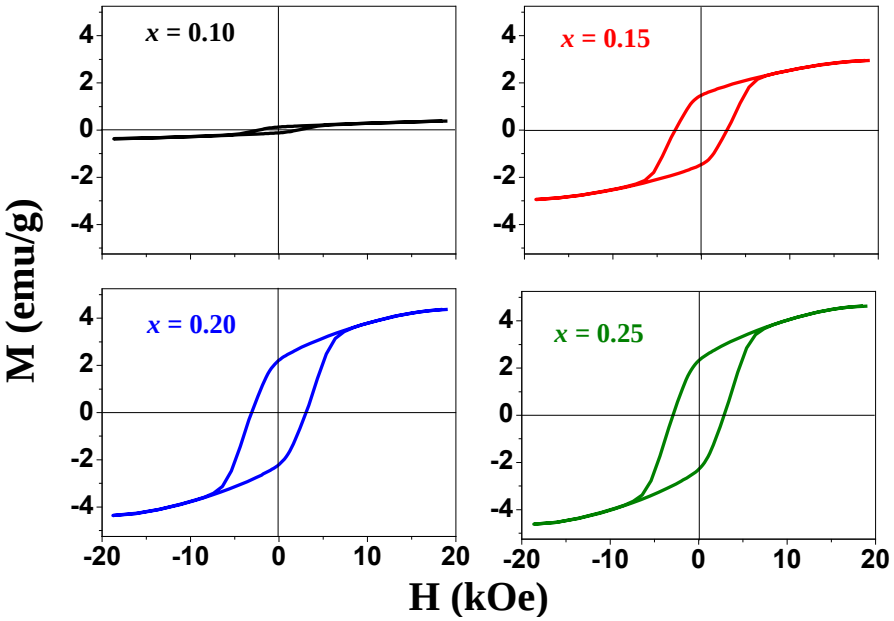

Fig.4 M–H hysteresis loops for $Bi_{1-x}Ba_xFeO_3$ multiferroic nanoparticles at room temperature.

Journal of. Modern Trends in Physics Research
Online ISSN 2636-4220
DOI: 10.19138/mtpr/(14)81-89
Accepted: 2014-12-19

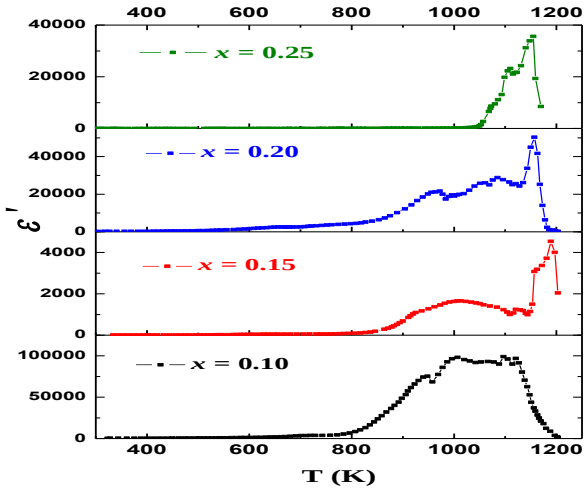

Fig. 5 Temperature dependence of dielectric constant (ε') for $Bi_{1-x}Ba_xFeO_3$ multiferroic nanoparticles at 300 kHz.

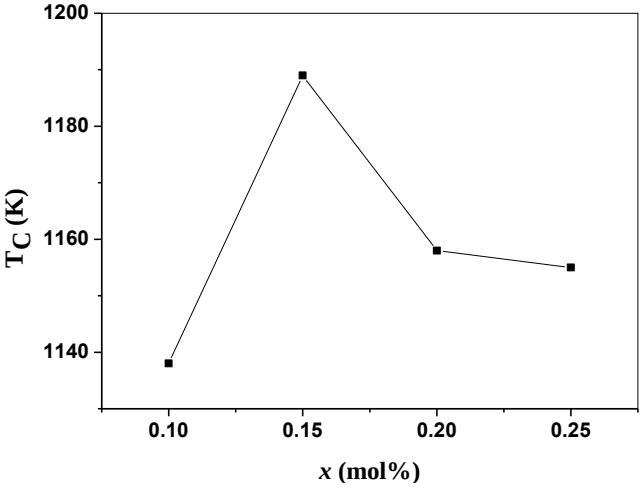

Fig. 6 Dependence of the Curie temperature (T_C) on the barium content (x).

Table 1. Particle size, lattice parameters and density of $Bi_{1-x}Ba_xFeO_3$ multiferroic nanoparticles at room temperature.

Sample	*D* ± 1 (nm)	*a* (Å)	*c* (Å)	*c/a*	*V* (Å^3)	*ρ* ± 0.01 (g/cm^3)
x = 0.10	33	5.609	13.673	2.438	372.50	8.17
x = 0.15	20	5.616	13.655	2.432	372.98	8.07
x = 0.20	23	5.621	13.713	2.440	375.15	7.93
x = 0.25	30	5.630	13.786	2.449	378.37	7.76

3. RESULTS AND DISCUSSIONS

Fig. 1 shows the X-ray diffraction (XRD) patterns for $Bi_{1-x}Ba_xFeO_3$ (x = 0.10, 0.15, 0.20 and 0.25 mol%) multiferroic nanoparticles at room temperature. As shown in Fig. 1, the appearance of strong reflection from (110), (024), (012), (214) and (202). The diffraction peaks of $BiBaFeO_3$ samples can be indexed to the rhombohedral–hexagonal structure (with space group R3c) which agrees with the results reported by Jaiparkash et al. [19]. Where the broad XRD peaks confirm that the samples are in nanocrystalline form. The average crystallite size of the nanoparticles has been calculated using the Debye–Scherrer equation

$$D = \frac{k\,\lambda}{\beta\,cos\theta}$$

where D is the crystallite size in Å, $k = 0.89$ is the correction factor, λ is the Cu target wavelength, β is the full width half maximum (FWHM) of the most intense peak and θ is the angle of diffraction. Small intensities of a secondary phases were observed for x = 0.10 mol%. These phases were indexed as $Bi_2Fe_4O_9$ and $BaFe_2O_4$ and with addition of Ba^{2+} ions; the impurity peaks of $Bi_2Fe_4O_9$ are vanished. To examine the effect of Ba^{2+} ions substitution on the structure, as can be seen clearly in the inset Fig. 1, with increasing Ba^{2+} ions substitution, the diffraction peaks of (104) and (110) merge to one peak for x = 0.15 mol%, indicating a structure phase transition from rhombohedral to hexagonal happens [19]. The average value of FWHM as shown from Fig. 1 has a maximum value at x = 0.15 mol%, it is indicating that the distortion in the system is maximum for x = 0.15 mol%. In addition, the crystallite size is small which change cycloidal spin structure to a canted spin structure [20–21]. The crystallite sizes of present samples are summarized in Table 1.

From XRD results, the lattice parameters (a and c) were computed based on hexagonal distortion of the rhombohedral unit cell with space group (R3c) and listed in Table 1 using the relation

Journal of. Modern Trends in Physics Research
Online ISSN 2636-4220
DOI: 10.19138/mtpr/(14)81-89
Accepted: 2014-12-19

$$\frac{1}{d^2} = \frac{4}{3}\frac{(h^2 + k^2 + hk)}{a^2} + \frac{l^2}{c^2}$$

where d is the inter-planar spacing and (h k l) are miller indices. It is clearly observed from the tabulated parameters that the lattice parameters increase slightly with increasing barium content obeying the well-known Vegard's law [22] and improvement in the volume (V) of the unit cell. The theoretical density (ρ) was calculated from the equation

$$\rho = \frac{ZM}{N_A V}$$

where Z is the number of molecules per unit cell, M is the molecular weight and N_A is the Avogadro's number [22]. It is clear that density decreases with increasing barium content. The density for these samples was consistent with the ionic size, atomic weight and amount of different elements in the samples as listed in Table 1.

Fig. 2 illustrates the relation between the molar magnetic susceptibility (χ_M) and absolute temperature (T), ranging from 300–1000 K at different magnetic field intensities (H). From the figure, it is observed that χ_M decreases with increasing temperature up to the Néel temperature (T_N). This decrease in χ_M is attributed to the thermal energy, which disturbs the oriented spins in the field direction. After reaching to the Néel temperature, the samples behave as a typical paramagnet. According to the relation $\chi_M = M/H$, molar magnetic susceptibility for all samples decreases with increasing magnetic field intensity as shown in Fig. 2. It is well-known that $BiFeO_3$ is a *G*–type antiferromagnetic material ordering with a cycloidal spin structure 620 Å apparent down to 5 K [23]. Where the dependence of magnetic properties on the direction in which they are measured is known as magnetic anisotropy [24]. The magnetic properties of $BiBaFeO_3$ depends on particle size because of long-range spin arrangement. Accordingly, the decrease in the particle size below the periodicity of cycloidal spin structure will enhance the magnetic properties. However, the weak ferromagnetic founding in $BiBaFeO_3$ originated from canting in the Fe^{3+} moments due to tilt of FeO_6 octahedron and the distortion can suppress the spiral spin structure and increase the weak ferromagnetism [13].

Fig. 3 illustrates the variation of Néel temperature (T_N) and crystallite size (D) as a function of barium content (x). As shown in Fig. 3, the result shows a decreasing trend with barium content up to x = 0.15 mol% and then increases to x = 0.25 mol%. This behavior could be explained on the basis of two factors, the first one is the change of Fe–O–Fe bond angles [25] because of phase transition from rhombohedral to hexagonal structure, structural distortion and oxygen vacancies. The second one is accordance with other size-dependent $BiFeO_3$ nanoparticles reports [26–27]. Due to the small particles size, the electron spins become fluctuated, this results in the Néel temperature decreasing when the size of particles decrease as the fluctuations create disorder. In addition, the reason may be related to the decrease of magnetic exchange interactions with reduction in particle size [27]. Also, from Fig. 3, the particle size and Néel temperature have the same trend as a function of barium content (x), which is desired for obtaining room temperature magnetoelectric coupling [26]. The maximum Néel temperature 834 K was found for x = 0.25 mol% with particle size 29 nm. Néel temperature (T_N) registers an increase of 30 times of Ba-doped $BiFeO_3$ in comparison with undoped $BiFeO_3$. The value of T_N was found to be larger than that reported for Ba-doped $BiFeO_3$ [7, 18, 28].

Table 2. Magnetic parameters of $Bi_{1-x}Ba_xFeO_3$ multiferroic nanoparticles at room temperature.

Sample	***H_c* (kOe)**	***M_r* (emu/g)**	***M_s* (emu/g)**	***M_r* / *M_s***
x = 0.10	2.24	0.12	0.38	0.328
x = 0.15	2.93	1.47	2.95	0.499
x = 0.20	3.06	2.21	4.36	0.507
x = 0.25	2.89	2.30	4.63	0.498

Fig. 4 shows the hysteresis loops of the $Bi_{1-x}Ba_xFeO_3$ (x = 0.10, 0.15, 0.20 and 0.25 mol%) multiferroic nanoparticles under an applied magnetic field at room temperature. It is clear that all samples exhibit a nonlinear magnetization dependence on magnetic field, nonzero remnant magnetization (M_r), saturation magnetization (M_s) and coercive field (H_c). Magnetic parameters are summarized in Table 2. The loop areas increased by increasing barium content, by meaning that the hysteresis loops tends to be square shape rather than *S*–shape. At x = 0.10, an almost linear behavior is obtained with a small values of M_r, M_s, H_c and a small loop area. In addition, it was found that an abrupt change, as

Journal of. Modern Trends in Physics Research
Online ISSN 2636-4220
DOI: 10.19138/mtpr/(14)81-89
Accepted: 2014-12-19

barium content increases, the values of M_r, M_s and H_c were increased. The reasons of enhancement ferromagnetic by increasing Ba^{2+} ions doping; i) an increase in the spin canting due to tilting of the FeO_6 octahedral [13]. ii) The substitution of divalent metal ions Ba^{2+} at trivalent Bi^{3+} sites requires oxygen deficiency for compensating charge and this may destabilize the system [29]. iii) It is expected to suppress the cycloid spin structure [30]. The small particle sizes observed in the samples of the order of 30 nm are excellent for efficient ferromagnetic properties, due to the magnetic cycloid spin structure of 62 nm in this material [31]. The maximum remnant magnetization M_r and saturation magnetization M_s were found for x = 0.25 mol% with particle size 29 nm as listed in Table 2. It is increased more than 18 times its initial value (x = 0.10 mol%).

The variation of real part of dielectric constant (ε') with the absolute temperature (T) from 300 K to 1200 K at 300 kHz for all samples is shown in Fig. 5. It clearly reveals that the general trend of all samples is the increase of ε' with increasing temperature up to Curie temperature (T_C). The increase of ε' take place depending on barium content due to replacing Bi^{3+} ions by Ba^{2+} ions will reduce the off center distortion because of Ba^{2+} ions does not have lone pair. Moreover, it is creating oxygen vacancies resulting in the collapse of oxygen octahedral FeO_6. At lower temperature, ε' increases slowly with temperature because of the weak contribution of electric dipoles to the polarization. With increasing temperature, ε' increases rapidly up to a maximum value. This increasing is due to the large number of dipoles that becomes free with high thermal energy and the field aligned them in its direction. The decrease in ε' values is due to thermal energy, which is too large and overcome the effect of the electric field. All samples have the same trend with different values of ε' and T_C.

Also, from the present samples, a dielectric anomaly in the ε'–T curve has been observed during the heating. The variation of abnormal peak position as a function of barium content is shown in Fig.5. The abnormal dielectric constant peak (intermediated range) around 1000 K, which appears in the vicinity of antiferromagnetic transition. Similar results have been observed in $Bi_{1-x}Ag_xFeO_3$, $BiFe_{0.75}Ti_{0.25}O_3$ and $BiFe_{1-x}Mn_xO_3$ multiferroic materials [32–34]. This type of abnormal dielectric demonstrates the coupling between the antiferromagnetic and dielectric properties as an influence of magnetic order transition on the electric order was predicted by the Landau–Devonshire theory [35]. The abnormal dielectric temperatures are higher than the antiferromagnetic transition and lower than the ferroelectric transition temperature. They should be related to the antiferromagnetic transition. The perovskite structure of $BiFeO_3$ results in two important considerations. First, the ferroelectric polarization lies along the pseudo-cubic <111> [36–37]. Second, the antiferromagnetic ordering oriented along the $[110]_c$ perpendicular to the ferroelectric polarization direction [36]. An antiferromagnetic transition from the spin-ordered state to the disordered state would effect on the ferroelastic state because of the strong coupling between the lattice strain and electronic structure gives rise to first order transition [38], then the ordered electric dipoles would be disturbed due to switching of the polarization is accompanied by switching of the ferroelastic domain state [33]. The intensity of the abnormal dielectric peak means that the coupling is strong. This strong coupling between electrical polarization and magnetic order is essential for a true multiferroic material system [35].

Fig. 6 illustrates the variation of Curie temperature (T_C) as a function of barium content (x). The maximum T_C =1189 K was found for x = 0.15 mol% as shown in Fig. 6. This maximum in Curie temperature may be attributed to phase transition from rhombohedral to hexagonal structure, doped with larger atoms [39]. On the other hand, the decrease in T_C with increasing barium content, this may be due to created oxygen vacancies in the system will lead to change and disordering the long–range ferroelectric order [40].

As can be seen in Fig. 7, the ferroelectric hysteresis loops (P–E) for all the samples $Bi_{1-x}Ba_xFeO_3$ (x = 0.10, 0.15, 0.20 and 0.25 mol%) multiferroic nanoparticles measured at fixed frequency (50 Hz) obtained at room temperature. All ferroelectric parameters coercive field (E_c), remnant polarization (P_r) and maximum polarization ($P_{max.}$) are summarized in Table 3. The loops for all samples exhibit an unsaturated hysteresis loops as shown in Fig. 7, there is not any loop has a rounded shape, which is due to decreasing leakage current [41]. From Table 3, it is clear that the maximum P_r = 88.8 μC/cm^2 was found for x = 0.15 mol% with $P_{max.}$ = 153.4 μC/cm^2. The enhancement of the polarization might be due to the fact that phase transition from rhombohedral to hexagonal structure and (c/a) ratio decreases with increase in barium content up to x = 0.15 mol% and then it increases considerably. From Fig. 7, it can be assumed that leakage current is negligible in all doped samples [28]. The value of polarization was found to be larger than that reported for Ba-doped $BiFeO_3$ [28, 35].

Journal of. Modern Trends in Physics Research
Online ISSN 2636-4220
DOI: 10.19138/mtpr/(14)81-89
Accepted: 2014-12-19

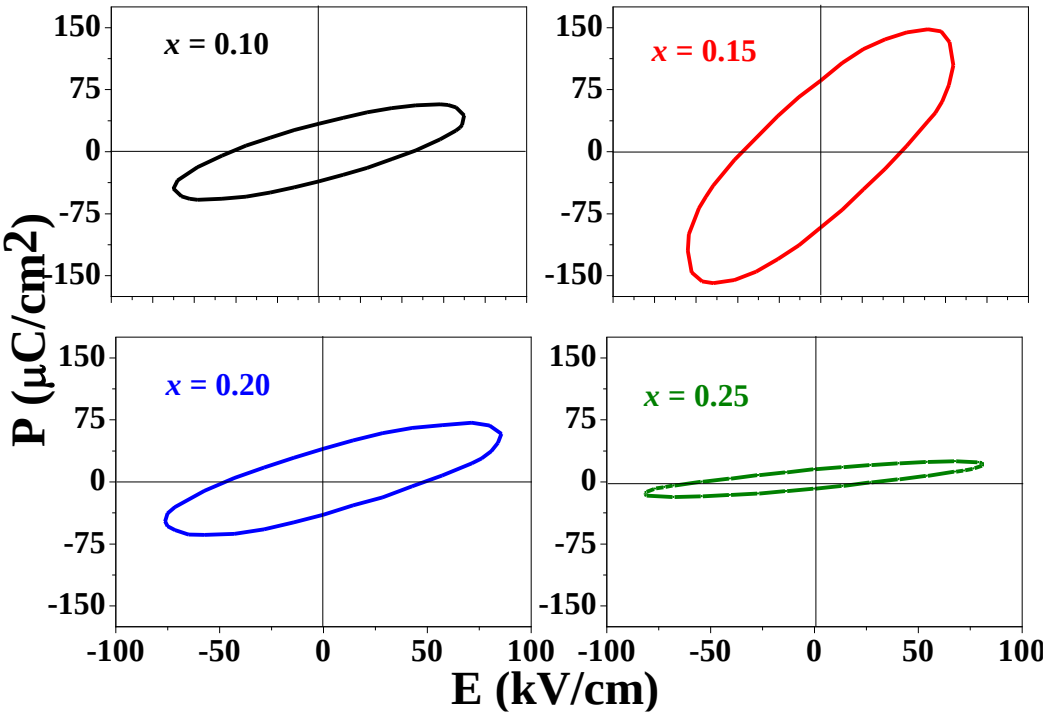

Fig.7 Ferroelectric hysteresis loops for $Bi_{1-x}Ba_xFeO_3$ multiferroic nanoparticles at room temperature.

Table 3. Ferroelectric parameters of $Bi_{1-x}Ba_xFeO_3$ multiferroic nanoparticles at room temperature.

Sample	E_c (kV/cm)	P_r (μC/cm^2)	$P_{max.}$ (μC/cm^2)	P_r / $P_{max.}$
x = 0.10	44.7	34.1	58.0	0.059
x = 0.15	37.9	88.8	153.4	0.579
x = 0.20	48.3	42.4	69.4	0.612
x = 0.25	42.8	11.4	21.3	0.538

4. CONCLUSION

We have succeeded in preparing $Bi_{1-x}Ba_xFeO_3$ (x = 0.10, 0.15, 0.20 and 0.25 mol%) multiferroic nanoparticles by solid-state reaction method. The lattice structure of the nanoparticles transformed from rhombohedral (x = 0.10 mol%) to hexagonal (x = 0.15, 0.20 and 0.25 mol%). By increasing barium content, the density decreased. Magnetic and ferroelectric properties of $BiFeO_3$ are found to change with Ba^{2+} ions substitution. Ba-doping transformed antiferromagnetic $BiFeO_3$ to ferromagnetic, and the magnetization was enhanced. An enhancement in ferromagnetic properties of $BiBaFeO_3$multiferroic nanoparticles for x = 0.25 mol% was observed with a remanent magnetization of 2.30 emu/g. For x = 0.25 mol%, there is more than 18 times increment in the value of remanent magnetization and approximately 30 times increment in magnetic transition T_N in comparison with undoped $BiFeO_3$. Best improvement of the magnetization was achieved at x = 0.25 mol%. In addition, an improvement in ferroelectric properties for x = 0.15 mol% was observed with a remanent polarization of 88.8 μC/cm^2. The maximum T_C = 1189 K was found for x = 0.15 mol%. Best enhancement of the ferroelectricity was found at x = 0.15 mol%. The dielectric properties of the samples were affected by the Ba^{2+} ions as well as the crystalline structure of the samples. The abnormal dielectric constant was observed, it demonstrates the coupling between the magnetic and dielectric properties. These results suggest that the $BiBaFeO_3$ nanoparticles are a good candidate for data storage applications. Finally, the simultaneous

Journal of. Modern Trends in Physics Research
Online ISSN 2636-4220
DOI: 10.19138/mtpr/(14)81-89
Accepted: 2014-12-19

occurrence of ferromagnetism and ferroelectric hysteresis loops in $BiBaFeO_3$ multiferroic nanoparticles system at room temperature makes it a potential candidate for information storage and spintronics.

5. REFERENCES

[1] K. Aizu. *Physical Review B* **2** (1970) 754–772.

[2] T. Kimura, S. Kawamoto, I. Yamada, M. Azuma, M. Takano, Y. Tokura. *Physical Review B* **67** (2003) 180401.

[3] N. Hur, S. Park, P. A. Sharma, J. S. Ahn, S. Guha, S. W. Cheong. *Nature* **429** (2004) 392–395.

[4] Y. H. Chu, L. W. Martin, M. B. Holcomb, M. Gajek, S. J. Han, Q. He, N. Balke, C. H. Yang, D. Lee, W. Hu, Q. Zhan, P. L. Yang, A. F. Rodríguez, A. Scholl, S. X. Wang, R. Ramesh. *Nature Materials* **7** (2008) 478–482.

[5] J. Wang, J. B. Neaton, H. Zheng, V. Nagarajan, S. B. Ogale, B. Liu, D. Viehland, V. Vaithyanathan, D. G. Schlom, U. V. Waghmare, N. A. Spaldin, K. M. Rabe, M. Wuttig, R. Ramesh. *Science* **299** (2003) 1719–1722.

[6] R. Ramesh, N. A. Spaldin. *Nature Materials* **6** (2007) 21–29.

[7] C. Yang, C. Z. Liu, C. M. Wang, W. G. Zhang, J. S. Jiang. *Journal of Magnetism and Magnetic Materials* **324** (2012) 1483–1487.

[8] J. R. Teague, R. Gerson, W. J. James. *Solid State Communications* **8** (1970) 1073–1074.

[9] B. Kundys, M. Viret, D. Colson, D. O. Kundys. *Nature Materials* **9** (2010) 803–805.

[10] G. Catalan, J. F. Scott. *Advanced Materials* **21** (2009) 2463–2485.

[11] A. K. Pradhan, K. Zhang, D. Hunter, J. B. Dadson, G. B. Loutts, P. Bhattacharya, R. Katiyar, J. Zhang, D. J. Sellmyer, U. N. Roy, Y. Chi, A. Burger. *Journal of Applied Physics* **97** (2005) 093903.

[12] R. Mazumder, P. S. Devi, D. Bhattacharya, P. Choudhury, A. Sen, M. Raja. *Applied Physics Letters* **91** (2007) 062510.

[13] M. A. Ahmed, E. Dhahri, S. I. El-Dek, M. S. Ayoub. *Solid State Sciences* **20** (2013) 23–28.

[14] Z. Wena, X. Shena, D. Wua, Q. Xub, J. Wangc, A. Li *Solid State Communications* **150** (2010) 2081–2084.

[15] A. Gautam, K. Singh, K. Sen, R. K. Kotnala, M. *Singh Materials Letters* **65** (2011) 591–594.

[16] D. S. García-Zaleta, A. M. Torres-Huerta, M. A. Domínguez-Crespo, J. A. Matutes-Aquino, A. M. González, M. E. Villafuerte-Castrejón. *Ceramics International* **40** (2014) 9225–9233.

[17] V. A. Khomchenko, D. A. Kiselev, E. K. Selezneva, J. M. Vieira, A. M. L. Lopes, Y. G. Pogorelov, J. P. Araujo, A. L. Kholkin. *Materials Letters* **62** (2008) 1927–1929.

[18] A. R. Makhdoom, M. J. Akhtar, M. A. Rafiq, M. M. Hassan. *Ceramics International* **38** (2012) 3829–3834.

[19] Jaiparkash, R. S. Chauhan, R. Kumar, Y. Kumar, N. Vijayan. *Journal of Alloys and Compounds* **598** (2014) 248–252.

[20] B. Yu, M. Li, J. Liu, D. Guo, L. Pei, X. Z. Zhao *Journal of Physics D Applied Physics* **41** (2008) 065003.

[21] J. W. Lin, Y. H. Tang, C. S. Lue, J. G. Lin. *Applied Physics Letters* **96** (2010) 232507.

[22] B. D. Cullity, Elements of X-ray Diffraction, second ed. *Addison-Wesley Publishing Company* 1978.

[23] Y. P. Wang, G. L. Yuan, X. Y. Chen, J-M. Liu, Z. G. Liu *Journal of Physics D Applied Physics* **39** (2006) 2019.

[24] S. Mandal, C. K. Ghosh, D. Sarkar, U. N. Maiti, K. K. Chattopadhyay. *Solid State Sciences* **12** (2010) 1803.

[25] M. Sivakumar, A. Gedanken, D. Bhattacharya, I. Brukental, Y. Yeshurun, W. Zhong, Y. W. Du, I. Felner, I. Nowik. *Chemistry of Materials* **16** (2004) 3623–3632.

[26] B. Bhushan, A. Basumallick, S. K. Bandopadhyay, N. Y. Vasanthacharya, D. Das *Journal of Physics D Applied Physics* **42** (2009) 065004.

[27] S. M. Selbach, T. Tybell, M. A. Einarsrud, T. Grande. *Chemistry of Materials* **19** (2007) 6478–6484.

[28] R. Das, K. Mandal. *Journal of Magnetism and Magnetic Materials* **324** (2012) 1913–1918.

[29] P. Godara, A. Agarwal, N. Ahlawat, S. Sanghi, R. Dahiya. *Journal of Alloys and Compounds* **594** (2014) 175–181.

[30] S. Hussain, S. K. Hasanain, G. H. Jaffari, N. Z. Ali, M. Siddique, S. I. Shah. *Journal of Alloys and Compounds* **622** (2015) 8–16.

[31] G. Rojas-George, J. Silva, R. Castañeda, D. Lardizábal, O. A. Graeve, L. Fuentes, A. Reyes-Rojas *Materials Chemistry and Physics* **146** (2014) 1–9.

[32] M. A. Ahmed, S. F. Mansour, S. I. El-Dek, M. Abu-Abdeen. *Materials Research Bulletin* **49** (2014) 352–359.

[33] M. Kumar, K. L. Yadav *Journal of Applied Physics* **100** (2006) 074111–074114.

[34] M. Kumar, K. L. Yadav. *Applied Physics Letters* **91** (2007) 242901–242903.

[35] M. S. Wu, Z. B. Huang, C. X. Han, S. L. Yuan, C. L. Lu, S. C. Xia *Solid State Communications* **152** (2012) 2142–2146.

[36] C. Ederer, N. A. Spaldin Physical Review B 71 (2005) 060401(R).

[37] F. Zavaliche, P. Shafer, R. Ramesh, M. P. Cruz, R. R. Das, D. M. Kim, C. B. Eom *Applied Physics Letters* **87** (2005) 182912.

[38] T. Maitra, P. Thalmeier, T. Chatterji *Physical Review B* **69** (2004) 132417.

[39] J. R. Sahu, C. N. *Rao Solid State Sciences* **9** (2007) 952–953.

[40] X. Xue, T. Guoqiang, R. Huijun, X. Ao. *Ceramics International* **39** (2013) 6223–6228.

[41] R. Rai, S. K. Mishra, N. K. Singh, S. Sharma, A. L. Kholkin *Current Applied Physics* **11** (2011) 508–512.

[42] H. Deng, M. Zhang, Z. Hu, Q. Xie, Q. Zhong, J. Wei, H. Yan. *Journal of Alloys and Compounds* **582** (2014) 273–276.